


 Cite this: *RSC Adv.*, 2022, 12, 365

# Germanium-based superatom clusters as excess electron compounds with significant static and dynamic NLO response; a DFT study†

 Atazaz Ahsin, Ahmed Bilal Shah  and Khurshid Ayub \*

Herein, the geometric, electronic, and nonlinear optical properties of excess electron zintl clusters  $\text{Ge}_5\text{AM}_3$ ,  $\text{Ge}_9\text{AM}_5$ , and  $\text{Ge}_{10}\text{AM}_3$  ( $\text{AM} = \text{Li}, \text{Na}, \text{and K}$ ) are investigated. The clusters under consideration demonstrate considerable electronic stability as well as superalkali characteristics. The NBO charge is transferred from the alkali metal to the Ge-atoms. The FMO analysis shows fabulous conductive properties with a significant reduction in SOMO–LUMO gaps (0.79–4.04 eV) as compared with undoped systems. The designed clusters are completely transparent in the deep UV-region and show absorption in the visible and near-IR region. Being excess electron compounds these clusters exhibit remarkable hyperpolarizability response up to  $8.99 \times 10^{-26}$  esu, where a static second hyperpolarizability ( $\gamma_{\text{d}}$ ) value of up to  $2.15 \times 10^{-30}$  esu was recorded for  $\text{Ge}_9\text{Na}_5$  superatom clusters. The excitation energy is the main controlling factor for hyperpolarizability as revealed from the two-level model study. The electro-optical Pockel's effect and the second harmonic generation phenomenon (SHG) are used to investigate dynamic nonlinear optical features. At a lower applied frequency ( $=532$  nm), the dynamic hyperpolarizability and second hyperpolarizability values are significantly higher for the studied clusters. Furthermore, for the  $\text{Ge}_9\text{K}_5$  cluster, the hyper Rayleigh scattering (HRS) increases to  $5.03 \times 10^{-26}$  esu.

 Received 8th November 2021  
 Accepted 4th December 2021

DOI: 10.1039/d1ra08192f

[rsc.li/rsc-advances](https://rsc.li/rsc-advances)

## 1 Introduction

The past several decades have witnessed increasing scientific and technology-driven interest in developing nonlinear optical (NLO) materials because of their tremendous importance in photonic applications.<sup>1,2</sup> The developments in the field of nonlinear optics and laser-based technologies started after the discovery of the ruby laser by Maiman in 1960.<sup>3</sup> Thus nonlinear optical materials have emerged rapidly during the last few decades, mainly due to their extensive applications in optoelectronic and photonic devices, second harmonic generation (SHG), endoscopy, and laser surgery<sup>4–8</sup> To date, numerous approaches for designing nonlinear optical materials with high hyperpolarizability have been used, including diradical character,<sup>9</sup> designing octupolar molecules,<sup>10</sup> the push–pull effect in conjugated chromophores,<sup>11</sup> multidecker sandwich complexes,<sup>12</sup> and excess electron models.<sup>13</sup> Among the studied nonlinear optical materials inorganic materials exhibit prime interest because of their physicochemical stability and thermal stability.<sup>14</sup>

The excess electron system is well-known for triggering second and third-order nonlinearity.<sup>15,16</sup> In the family of excess

electron compounds, electride,<sup>17</sup> alkalides,<sup>18</sup> and alkaline-earthides<sup>19,20</sup> are well known.

Electrides are compounds in which electron trapping into the complexant acts as an anion.<sup>21</sup> Similarly, the alkalides are compounds in which alkali metals possess a negative charge and become anion ( $\text{Li}^-$ ,  $\text{Na}^-$ ,  $\text{K}^-$ ).<sup>22</sup> Alkaline-earthides are also a fabulous excess electron system that contains a negative charge on alkaline-earth metals ( $\text{Be}^-$ ,  $\text{Mg}^-$ ,  $\text{Ca}^-$ ).<sup>23</sup> Excess electron compounds can be designed by doping any complexant with alkali metals,<sup>24,25</sup> alkaline earth metals,<sup>26</sup> transition metals<sup>27,28</sup> and superalkali clusters.<sup>29,30</sup>

Superalkali clusters belong to the superatom clusters family and exhibit alkali-like characteristics with tunability in their electronic and geometric properties.<sup>31</sup> The term ‘superalkalis’ was first time introduced by Gutsev and Boldyrev for  $\text{Li}_3\text{O}$ ,  $\text{Li}_2\text{F}$ ,  $\text{NLi}_4$  etc. through DVM $\alpha$  calculations. The superalkali clusters materials are of prime interest and show significant applications in numerous fields including, catalysis,<sup>32</sup> reduction of  $\text{CO}_2$  and  $\text{N}_2$ ,<sup>33</sup> hydrogen storage materials, and nonlinear optics.<sup>34</sup> Thus, being excess electron compounds superalkali clusters can be adopted for making high-performance nonlinear optical materials. Furthermore, several studies have been proposed that reveal that superalkali being excess electron clusters can be doped with different molecules and nanocages to form excess electron compounds for triggering the NLO response. In this regard, superalkali-doped nanocages  $\text{Li}_3\text{O}@\text{Al}_{12}\text{N}_{12}$  were theoretically designed with electride characteristics for enhanced

Department of Chemistry, COMSATS University Islamabad, Abbottabad Campus, Abbottabad, KPK, 22060, Pakistan. E-mail: khurshid@cuiatd.edu.pk

† Electronic supplementary information (ESI) available. See DOI: 10.1039/d1ra08192f



nonlinear optical response.<sup>35</sup> Similarly, superalkali doped 2D graphdiyne  $M_2X@GDY$  (where  $M = Li, Na, K$ , and  $X = F, Cl, Br$ ) were studied, and it was observed that there is a significant decrease in the HOMO–LUMO gap with a noticeable increase in hyperpolarizability response.<sup>36</sup> Moreover, superalkali clusters were doped with different 2D materials and nanocages to get excess electron compounds *i.e.* alkali, alkaline earths. These excess electron compounds were reported as excellent nonlinear optical materials with significant hyperpolarizability.<sup>24,37,38</sup> However, a very limited number of studies were reported that reveal the nonlinear optical response of pure superalkali clusters as efficient nonlinear optical materials.

A few number of pure superalkali clusters are investigated as excess electron compounds and show remarkable hyperpolarizability. In this regard, Misra *et al.*, investigated the electronic and nonlinear optical response of hyper lithiated superalkali clusters and reported these clusters as efficient NLO materials. The nonlinear optical response increases up to  $1.2 \times 10^4$  au.<sup>39</sup> Subsequently, another class of superalkali clusters  $CNLi_n$  ( $n = 1-10$ ) was investigated for nonlinear optical response and second-order NLO response was much pronounced.<sup>40</sup> The literature reveals that only conventional types of superalkali clusters are explored for optical and nonlinear optical studies however several models can be efficiently utilized to be used as nonlinear optical responses. Literature also reveals, there are several superatom clusters (silicon-based) encapsulated by transition metals which were also studied for optical and magnetic excitation<sup>41,42</sup>

Zintl polyanions, discovered by Eduard zintl in 1930 belong to the group (14,15) and show excellent physicochemical stability.<sup>43</sup> It is previously reported that zintl  $P_7^{3-}$  anion as core material can be used to design organo-zintl superalkali clusters which contain superb electron properties.<sup>44</sup> Similarly, zintl based superalkalis as a building block, when treated with superhalogens make novel supersalt compounds with significant electronic and nonlinear optical properties.<sup>45</sup> Moreover, superalkali clusters other than alkali metals might possess better stability and a high nonlinear optical response. We become interested in zintl-based superatoms, particularly germanium-based superatoms (which belong to group 14 elements) for electronic and optical properties. Furthermore, the stoichiometry of these clusters obeys magic number nuclei, in which their valence shells are organised as 1S2, 1P6, 1D10, 2S2, 1F14 after losing one electron, achieving electronic shell closure (according to Jellium model). When designed with alkali metals, Ge semimetallic clusters may have improved optoelectronic and NLO features. Although the  $Ge_5Li_3$ ,  $Ge_9Li_5$ , and  $Ge_{10}Li_3$  were theoretically studied by Sun *et al.*<sup>46</sup> Their investigations were limited to electronic properties whereas we adopted the alkali decorated zintl clusters  $Ge_5AM_3$ ,  $Ge_9AM_5$  and  $Ge_{10}AM_5$  (where  $AM = Li, Na, K$ ) for exploring optoelectronic and nonlinear optical properties.

In these studied clusters, we are mainly concerned with the following issues. Do these clusters belong to superalkali with better thermal and electronic stability than conventional superalkalis do these clusters possess nonlinear optical responses for declaring them as efficient NLO materials. The NLO response was confirmed by hyperpolarizability calculation and second hyperpolarizability.

## 2 Computational details

Initially, all the studied alkali decorated zintl polyanions  $Ge_5AM_3$ ,  $Ge_9AM_5$ , and  $Ge_{10}AM_3$  (where  $AM = Li, Na, K$ ) are considered and optimized at CAM-B3LYP/6-311+G(d,p) level of theory. The geometries of  $Ge_5Li_3$ ,  $Ge_9Li_5$ , and  $Ge_{10}Li_3$  were reported in the previous literature and we adopted the similar design for the rest of the alkali metals.<sup>46</sup> All the calculations were performed with Gaussian 09 software.<sup>47</sup> The CAM-B3LYP (Coulomb attenuating method) is a hybrid exchange–correlation functional that includes the hybrid properties of B3LYP functional and long-range corrected Coulomb-Attenuating Method (CAM).<sup>48</sup> B3LYP is a hybrid part of the above method that contains Beckes 3-parameters for exchange functional and Lee–Yang–Parr-correlation functional. This hybrid density functional theory-based method comprises 0.19 HF plus 0.81 (B88) exchange interactions at short range and 0.65 HF plus 0.35 (B88) long-range interactions.<sup>49</sup> The CAM-B3LYP is a well-known approach for linear and nonlinear optical characteristics of various clustered materials, and it has already been demonstrated to give appropriate geometries and comparable hyperpolarizability values with CCDST.<sup>50–53</sup> Besides, the triple zeta split valence basis set 6-311+G(d,p) with diffuse and polarized function is adopted throughout the calculations.

To explore the electronic stabilities of these clusters, we calculated vertical ionization potential and electron affinity.

$$IE = E_X^+ - E_X^0 \quad (1)$$

$$EA = E_X^- - E_X^0 \quad (2)$$

The chemical hardness is also calculated to understand their reactivity and soft nature and given by equation below<sup>54</sup>

$$\text{Chemical hardness } (\eta) = VIP - VEA \quad (3)$$

To further explore the electronic properties, we performed frontier molecular orbital (FMOs) analysis which included SOMO, LUMO, and  $E_{H-L}$  gap. The FMOs analysis also provides evidence of the excess electron nature of studied superalkali clusters. Natural bonding orbitals (NBO) study is conducted to explore the nature and charge distribution as studied superatom clusters. The time-dependent density functional (TD-DFT) theory is adopted to calculate the excited state parameters and absorbance behavior of studied zintl superatom clusters. The time-dependent density functional (TD-DFT) is well known for obtaining excited states parameters and absorption spectra of molecules and clusters. The TD-DFT was chosen because of its performance and its correspondence to experimental results. For this purpose excited-state calculations with TD-CAM-B3LYP/6-311+G(d,p) are performed. Mathematically system under the constant field can be expressed as:

$$E(F) = E^0 - \mu_i F_i - \frac{1}{2} \alpha_{ij} F_i F_j - \frac{1}{6} \beta_{ijk} F_i F_j F_k - \frac{1}{24} \gamma_{ijkl} F_i F_j F_k F_l \dots \quad (4)$$



where  $F$  is an external applied electric field on the molecular system,  $F_i$  is its component of force along  $i$  direction;  $E^0$  is the total energy of the superalkali clusters without a static electric field,  $\mu_i$ ,  $\alpha_{ij}$ ,  $\beta_{ijk}$ , and  $\gamma_{ijkl}$  are dipole moment, polarizability, hyperpolarizability, and second-order hyperpolarizability, respectively. Thus regarding nonlinear optical properties, the following parameters are estimated including the mean dipole moment ( $\mu_o$ ), change in dipole moment ( $\Delta\mu$ ), static polarizability ( $\alpha$ ) and static first hyperpolarizability ( $\beta$ ).

$$\alpha_o = 1/3(\alpha_{xx} + \alpha_{yy} + \alpha_{zz}) \quad (5)$$

$$\beta_o = \sqrt{\beta_x^2 + \beta_y^2 + \beta_z^2} \quad (6)$$

where  $\beta_x = \beta_{xxx} + \beta_{xyy} + \beta_{xzz}$ ,  $\beta_y = \beta_{yyy} + \beta_{yzz} + \beta_{yxx}$  and  $\beta_z = \beta_{zzz} + \beta_{zxx} + \beta_{zyy}$ .

$$\mu_o = (\mu_x^2 + \mu_y^2 + \mu_z^2)^{1/2} \quad (7)$$

Besides, the second static hyperpolarizability ( $\gamma_o$ ) and the projection of hyperpolarizability on the dipole moment vector ( $\beta_{vec}$ ) is also calculated for our studied superalkali clusters at the same level of theory. Vector part of hyperpolarizability ( $\beta_{vec}$ ) and second hyperpolarizability ( $\gamma$ ) are expressed defined as

$$\langle \gamma \rangle = 1/5(\gamma_{xxxx} + \gamma_{yyyy} + \gamma_{zzzz} + \gamma_{xxyy} + \gamma_{xxzz} + \gamma_{yyxx} + \gamma_{yyzz} + \gamma_{zzxx}) \quad (8)$$

$$\beta_{vec} = \sum \frac{\mu_i \beta_i}{|\mu|} \quad (9)$$

Mathematically  $\beta_{HRS}$  can be expressed as;

$$\beta_{HRS}(-2\omega; \omega, \omega) = \sqrt{\langle \beta_{zzz}^2 \rangle + \langle \beta_{zxx}^2 \rangle} \quad (10)$$

where  $\langle \beta_{zzz}^2 \rangle$  and  $\langle \beta_{zxx}^2 \rangle$  are average of orientational ( $\beta$ ) tensor.

While the related depolarization ratio for these superalkali clusters (DR) ratio is also given by;

$$DR = \langle \beta_{zzz}^2 \rangle / \langle \beta_{zxx}^2 \rangle$$

The frequency-dependent NLO analysis was conducted at 532 and 1064 nm wavelength. Frequency-dependent hyperpolarizability involves the electro-optic Pockel's effect (EOPE)  $\beta(-\omega; \omega, 0)$  and electric field induced second harmonic generation (ESHG)  $\beta(-2\omega; \omega, \omega)$  respectively. While for second hyperpolarizability ( $\gamma$ ), dc-Kerr  $\gamma^{dc-Kerr}(\omega) = \gamma(-\omega; \omega, 0, 0)$  and second harmonic generation  $\gamma^{ESHG}(\omega) = \gamma(-2\omega; \omega, \omega, 0)$  were considered.

## 3 Results and discussion

### 3.1 Geometries and electronic properties

All the optimized geometries of  $Ge_5AM_3$ ,  $Ge_9AM_5$ , and  $Ge_{10}AM_3$  (where AM = Li, Na, K) zintl superalkali clusters and their equilibrium bond length are depicted in Fig. 1. The geometric

parameters of these clusters are identical to those reported in the earlier literature<sup>46</sup> and are included in the ESI† (S1).

These clusters have no imaginary frequency (negative frequency) according to the frequency calculations, hence they are true minima on the potential energy surface (PES).

The computed ionization potential and electron affinity are used to analyze the electronic stability and superalkali nature of the investigated clusters. The difference in ground state energy between the cationic and neutral systems is described as the ionization potential (IP), meanwhile, the difference in ground state energy between the neutral and anionic systems is defined as the electron affinity.

The vertical ionization potential (VIP) values for  $Ge_9AM_3$  are in the range of 5.49 to 3.91 eV, and it decreased dramatically as the alkali-metal size rose (Li to k). The VIP values for the  $Ge_9AM_5$  series follow a similar pattern, reaching to 2.15 eV for F (Table 1). On the other hand, the VIP values for  $Ge_{10}AM_3$  are slightly higher than for  $Ge_9AM_5$  (Table 1). The lower VIPs values for the  $Ge_9AM_5$  series can be attributed to the higher number of alkali metals (AM = 5), which is responsible for the cluster's electro-positive nature. Additionally, their superalkali nature is demonstrated by their relatively low ionization potential values than Li atoms (5.4 eV).

The calculated vertical electron affinity (VEA) values of these superalkali clusters range from 0.02 to 1.15 eV. In the designed series,  $Ge_9AM_5$  has a smaller VEA value than those of  $Ge_3AM_3$  and  $Ge_{10}AM_3$ . The electro-positive feature of the examined superalkalis is revealed by the tiny VEA values. Furthermore, the reduced VEA values indicate that these alkali-decorated zintl clusters are unable to completely grasp the valence (loosely bound) electron, which could result in interesting electrical properties. Table 1 shows that the examined clusters are polarizable and soft, based on the computed minimal values of chemical hardness. The calculated chemical hardness ( $\eta$ ) values decrease with increased alkali metals size within these clusters. Among the series,  $Ge_9AM_5$  clusters shows lower values of chemical hardness which may be attributed to the higher number of alkali smaller metals (soft) in these clusters.

### 3.2 Natural bonding orbital (NBO) analysis

The NBO analysis is a useful tool for interpreting intramolecular and intermolecular interactions and conjugative interactions in compounds and clusters.<sup>55</sup> For  $Ge_5AM_3$  clusters, the obtained charges on alkali metals (QAM) vary from 0.86 to 0.90|e| (positive magnitude). The C cluster has the highest computed positive charge of 0.90|e|, while A has the lowest value of 0.86|e| in the  $Ge_5AM_3$  family. Similarly, the  $Ge_9AM_5$  clusters, computed average charge (QAM) ranges from 0.85 to 0.90|e| (Table 1). For the  $Ge_{10}AM_3$  superalkali clusters, similar NBO (positive magnitude) charges are observed. Hence, the computed positive NBO charges upon alkali metals shows the significant charge transfer (from alkali metals to Ge-atom) within the superalkali clusters. Additionally, the computed NBO charges upon germanium metals ( $Q_{Ge}$ ) for  $Ge_5AM_3$  range from  $-0.13$  to  $-0.69$ |e| (negative in magnitude). Therefore from the computed NBO charges (Table 1) one can observe the excellent separation of



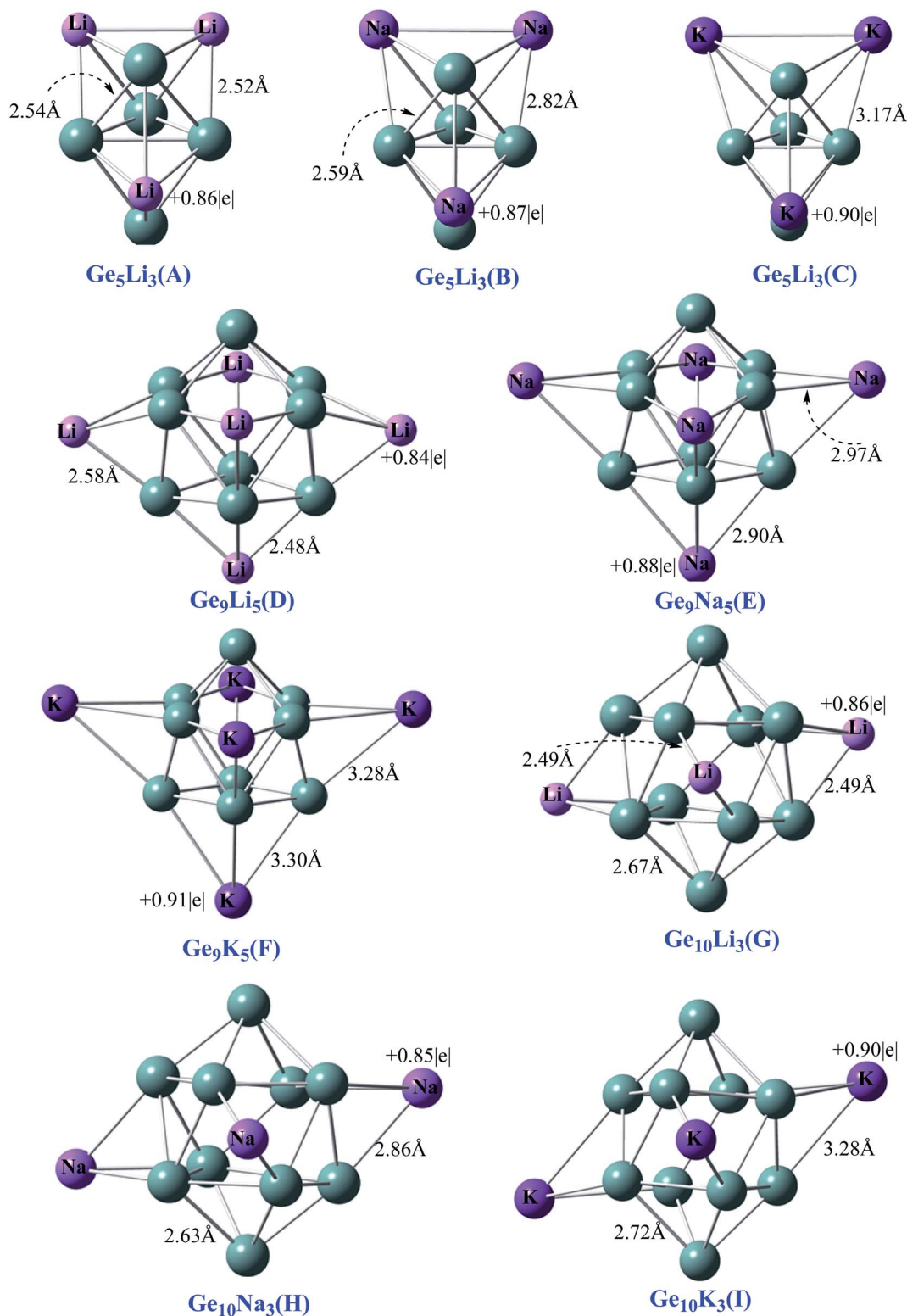


Fig. 1 Optimized geometries with NBO charge of  $\text{Ge}_5\text{AM}_3$ ,  $\text{Ge}_9\text{AM}_5$  and  $\text{Ge}_{10}\text{AM}_3$  clusters.

charges within the clusters. Likewise, the computed NBO charges ( $Q_{\text{Ge}}$ ) for the  $\text{Ge}_9\text{AM}_3$  clusters are range from  $-0.09$  to  $-0.61|e|$  where the highest value of  $-0.61|e|$  is obtained for  $\text{Ge}_9\text{Li}_5$  while the lowest value ( $-0.50$ ) is obtained for  $\text{Ge}_9\text{K}_5$

superalkali. However, the reported NBO charges ( $Q_{\text{Ge}}$ ) for the third series  $\text{Ge}_{10}\text{AM}_3$  are reduced (in negative magnitude) with corresponding increased cluster size. The overall NBO charges is an order of  $\text{Ge}_5\text{AM}_3 > \text{Ge}_9\text{AM}_5 > \text{Ge}_{10}\text{AM}_3$ .



**Table 1** Vertical ionization potential (VIP, in eV), vertical electron affinity (VEA in eV), maximum chemical hardness ( $\eta$  in eV), average NBO charge upon germanium ( $Q_{\text{Ge}}$  in  $|e|$ ), an average charge upon alkali metal ( $Q_{\text{AM}}$  in  $|e|$ ), of  $\text{Ge}_5\text{AM}_3$ ,  $\text{Ge}_9\text{AM}_5$  and  $\text{Ge}_{10}\text{AM}_3$  (where AM = Li, Na, K)

Superalkalis	VIP	VEA	$\eta$	$Q_{\text{Ge}}$	$Q_{\text{AM}}$
<b><math>\text{Ge}_5\text{AM}_3</math> (where AM = Li, Na, K)</b>					
$\text{Ge}_5\text{Li}_3$ (A)	5.49	0.98	4.51	−0.69	0.86
$\text{Ge}_5\text{Na}_3$ (B)	4.69	0.64	4.05	−0.65	0.87
$\text{Ge}_5\text{K}_3$ (C)	3.91	0.29	3.62	−0.65	0.90
<b><math>\text{Ge}_9\text{AM}_5</math></b>					
$\text{Ge}_9\text{Li}_5$ (D)	4.36	0.65	3.71	−0.61	0.85
$\text{Ge}_9\text{Na}_5$ (E)	2.81	0.07	2.74	−0.52	0.88
$\text{Ge}_9\text{K}_5$ (F)	2.15	0.02	2.13	−0.50	0.90
<b><math>\text{Ge}_{10}\text{AM}_3</math></b>					
$\text{Ge}_{10}\text{Li}_3$ (G)	4.98	1.15	3.83	−0.38	0.86
$\text{Ge}_{10}\text{Na}_3$ (H)	4.34	0.67	3.67	−0.36	0.85
$\text{Ge}_{10}\text{K}_3$ (I)	3.50	0.11	3.39	−0.46	0.90

### 3.3 Frontier molecular orbital (FMO) analysis and excess electron character

FMO analysis is adopted to validate the reactivity of the studied cluster system. Thus according to the frontier molecular orbital treatment of chemical reactivity, the rate, and site of reactivity of a molecule with a nucleophile is dominated by the interaction of the LUMO of the molecule in question with the HOMO of the nucleophile. The closer these orbitals are in energy, the more intensely they will interact, and the higher is the reactivity will be. Result in Table 2 show that the computed values for singly occupied molecular orbitals (SOMO), LUMO, and  $E_{\text{S-L}}$  gaps. For the  $\text{Ge}_5\text{AM}_3$ , the obtained values of singly occupied molecular orbitals (SOMO) vary from −4.99 to −3.51 eV and increase from A to C. For  $\text{Ge}_9\text{AM}_5$ , predicted SOMO energies are in the range of −3.97 to −1.80 eV, as well. The  $\text{Ge}_{10}\text{AM}_3$  clusters, on the other hand, have lower SOMO energies than those of  $\text{Ge}_9\text{AM}_5$  clusters, and these range from −4.46 to −3.14 eV. It can also be concluded that the SOMO energies of the examined superalkali clusters rise monotonically as the size of the alkali metals increases. Thus the observed trend of SOMO energies for studied superalkali clusters is  $\text{Ge}_9\text{AM}_5 < \text{Ge}_{10}\text{AM}_3 < \text{Ge}_5\text{AM}_3$ . Furthermore, the estimated LUMO energies for  $\text{Ge}_5\text{AM}_3$  clusters vary with cluster size. However, the estimated energies of virtual orbitals for the  $\text{Ge}_9\text{AM}_5$  series are increasing, while the  $\text{Ge}_{10}\text{AM}_3$  clusters are increasing even high.

For  $\text{Ge}_5\text{AM}_3$  clusters, there is a considerable reduction in the SOMO–LUMO gap, with values ranging from 4.06 to 2.77 eV. The HOMO–LUMO gaps for  $\text{Ge}_5\text{AM}_3$  clusters are around 4.06 to 2.77 eV, indicating that these compounds behave like semiconductors. Similarly, the observed reduction in  $\text{Ge}_9\text{AM}_5$   $E_{\text{H-L}}$  values from 3.89 to 0.79 eV could be attributable to their higher SOMO energies. Furthermore, the  $\text{Ge}_{10}\text{AM}_3$  series' HOMO–LUMO gap values are slightly higher than the  $\text{Ge}_9\text{AM}_5$  series, and range from 3.37 to 2.45 eV (Table 2). The significant reduction in HOMO–LUMO gaps reveals the soft nature (higher reactivity) and conductive properties of these clusters.

**Table 2** Energies of SOMO and LUMOs (in eV), HOMO–LUMO gaps ( $E_{\text{H-L}}$  in eV), excitation energies ( $\Delta E$  in eV), the wavelength of maximum absorbance ( $\lambda_{\text{max}}$  in nm), oscillator strength ( $f_o$  in au), ground-state dipole moment ( $\mu_o$  in au), and excited-state dipole moment ( $\Delta\mu$  in au) of  $\text{Ge}_5\text{AM}_3$ ,  $\text{Ge}_9\text{AM}_5$  and  $\text{Ge}_{10}\text{AM}_3$  superalkali clusters

Superalkalis	SOMO	LUMO	$E_{\text{H-L}}$	$\Delta E$	$\lambda_{\text{max}}$	$f_o$	$\mu$	$\Delta\mu$
<b><math>\text{Ge}_5\text{AM}_3</math> (where AM = Li, Na, K)</b>								
$\text{Ge}_5\text{Li}_3$ (A)	−4.99	−0.94	4.04	2.16	571	0.015	1.63	1.05
$\text{Ge}_5\text{Na}_3$ (B)	−4.24	−0.99	3.25	2.16	572	0.015	2.26	1.14
$\text{Ge}_5\text{K}_3$ (C)	−3.51	−0.73	2.77	2.24	553	0.041	3.12	2.34
<b><math>\text{Ge}_9\text{AM}_5</math></b>								
$\text{Ge}_9\text{Li}_5$ (D)	−3.97	−0.07	3.89	2.25	548	0.007	0.27	0.62
$\text{Ge}_9\text{Na}_5$ (E)	−2.42	−1.07	1.34	1.77	688	0.076	1.69	2.49
$\text{Ge}_9\text{K}_5$ (F)	−1.80	−1.02	0.79	1.12	1101	0.219	2.21	1.86
<b><math>\text{Ge}_{10}\text{AM}_3</math></b>								
$\text{Ge}_{10}\text{Li}_3$ (G)	−4.40	−0.87	3.73	2.31	534	0.007	1.45	0.62
$\text{Ge}_{10}\text{Na}_3$ (H)	−4.00	−0.83	3.16	2.47	500	0.008	1.55	0.65
$\text{Ge}_{10}\text{K}_3$ (I)	−3.14	−0.69	2.45	2.14	578	0.005	1.67	0.49

Furthermore, the observed reduced SOMO–LUMO gap within clusters is attributed to the larger size of alkali metals (ease in the transition of electron from occupied to virtual orbitals).

Moreover, the excess electron character of clusters can be seen in the electronic density distribution (Fig. 2). The excess electron cloud is indicated by the electronic density of SOMO and LUMO scattered throughout the alkali metals that resemble to s-orbital. The LUMO electronic density for  $\text{Ge}_{10}\text{AM}_3$  clusters wraps around the alkali metals, whereas the LUMO densities for  $\text{Ge}_9\text{AM}_5$  clusters move away from the alkali metals.

### 3.4 TD-DFT analysis of clusters

Time-dependent density functional theory was used to examine the absorbance behavior of  $\text{Ge}_5\text{AM}_3$ ,  $\text{Ge}_9\text{AM}_5$ , and  $\text{Ge}_{10}\text{AM}_3$  superalkali clusters. For nonlinear optical applications, the cluster materials employed should be transparent in the used region. In the absorption study, we calculated the maximum absorbance, excitation energy, and oscillator strength (during the electronic transition). The computed excited state parameters for the studied superalkali clusters are given in Table 2. From the computed results one can observe that the studied clusters are completely transparent in the UV-region (<400 nm) and show broadband absorbance in the visible region. The longer absorbance wavelength for the  $\text{Ge}_5\text{AM}_3$  ( $\lambda_{\text{max}} = 572$  nm) is observed for the  $\text{Ge}_5\text{Na}_3$  superalkali cluster whereas the lowest absorbance maxima ( $\lambda_{\text{max}} = 553$  nm) is obtained for the  $\text{Ge}_5\text{K}_3$  superalkali cluster (Fig. 3). However, the  $\text{Ge}_9\text{AM}_5$  series shows higher absorbance maxima ( $\lambda_{\text{max}} = 1101$  nm) for  $\text{Ge}_9\text{K}_5$  clusters. Similarly, for the second series, the highest absorbance maxima ( $\lambda_{\text{max}} = 578$  nm) is observed for the  $\text{Ge}_{10}\text{K}_3$  cluster in the  $\text{Ge}_{10}\text{AM}_3$  series. Overall, the clusters of  $\text{Ge}_9\text{AM}_5$  series shows absorption maxima at a longer wavelength (bathochromic shift) whereas the  $\text{Ge}_5\text{AM}_3$  and  $\text{Ge}_{10}\text{AM}_3$  have slightly blue-shifted wavelengths. As a result of their total transparency under deep UV-region, the optoelectronic properties of the examined



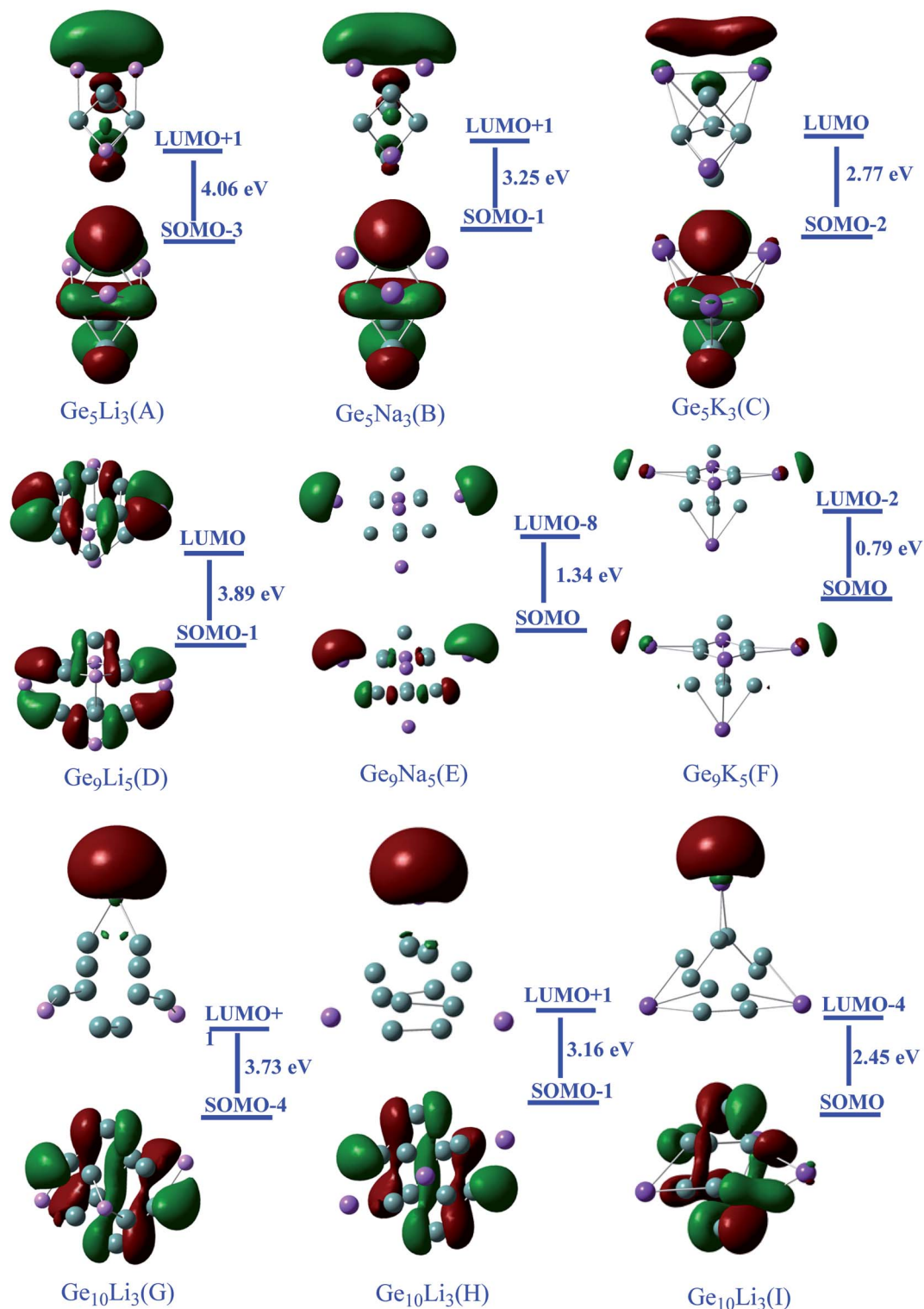


Fig. 2 Representation of Frontier molecular orbital densities along with orbitals contribution of superalkali clusters (*iso*-value of 0.030).

clusters fall under the UV-region. Furthermore, the excitation energies ( $\Delta E$ ) of Ge<sub>5</sub>AM<sub>3</sub> (*i.e.* excitation of an electron from HOMO to LUMO) are also very small and ranges from 2.16 to 2.24 eV whereas the observed excitation energies ( $\Delta E$ ) for the Ge<sub>9</sub>AM<sub>5</sub> are further reduced and lie in the range of 1.12 to

2.25 eV. Alternatively, the computed excitation energies of the Ge<sub>10</sub>AM<sub>3</sub> series are slightly higher than those of Ge<sub>9</sub>AM<sub>5</sub> and display a range of 2.14 to 2.47 eV. Moreover, the calculated oscillator strength (probability of absorbance during excitation) shows significant values for Ge<sub>5</sub>AM<sub>3</sub> superalkali clusters while



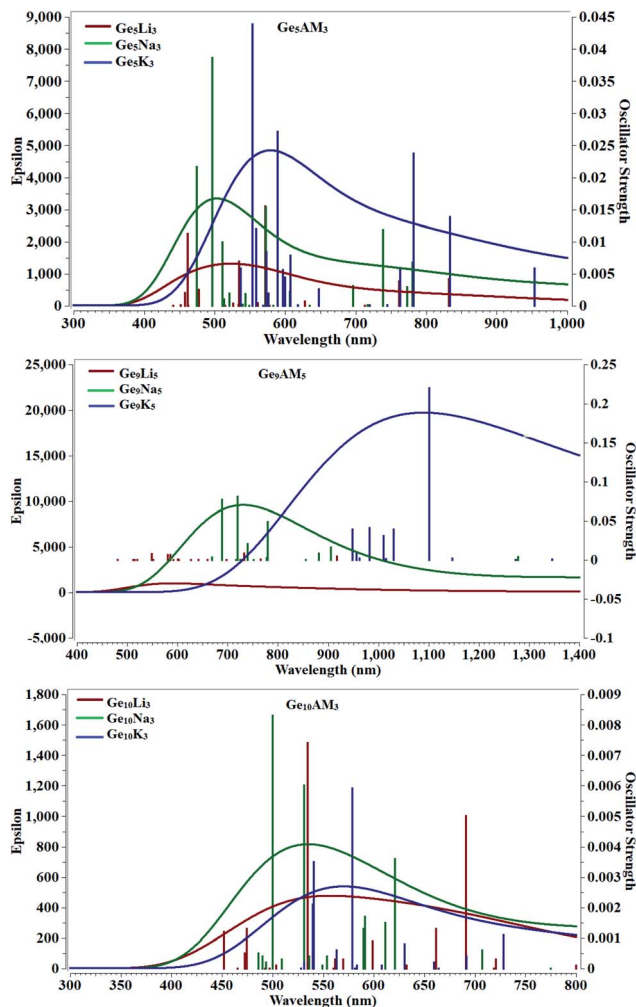


Fig. 3 Absorbance spectra of  $\text{Ge}_5\text{AM}_3$ ,  $\text{Ge}_9\text{AM}_5$ , and  $\text{Ge}_{10}\text{AM}_3$ .

the  $\text{Ge}_9\text{AM}_5$  and  $\text{Ge}_{10}\text{AM}_3$  have slightly reduced values of oscillator strength ( $f_o$ ).

### 3.5 Dipole moment and change in dipole moment

Table 2 shows the computed values of mean dipole moment ( $\mu_o$ ) and change in dipole moment ( $\Delta\mu$ ). The magnitude of polarisation in clusters and the asymmetric charge distribution are shown by the significant values of dipole moments. For the  $\text{Ge}_5\text{AM}_3$  series, the observed mean dipole moments range from 1.63 to 3.13 au. As the size of alkali metals grows larger (Li to K), the dipole moment gradually increases. Likewise, the calculated values of the dipole moment of  $\text{Ge}_9\text{AM}_5$  range from 0.27 to 2.21 au. Thus the calculated values of dipole moment for the  $\text{Ge}_9\text{AM}_5$  are slightly smaller than those of  $\text{Ge}_5\text{AM}_3$  clusters. On the other hand, the computed mean dipole moments are enhanced for the  $\text{Ge}_{10}\text{AM}_3$  series and the values lie in the range of 1.42 to 1.67 au. Hence, from the computed results, one can conclude that a significant dipole moment that is associated with the  $\text{Ge}_5\text{AM}_3$  series would result in larger polarization. Our calculations also show that the studied alkali decorated zintl polyanions clusters possess polar bonds (asymmetric electronic density) that might

be an important factor for imparting optical and nonlinear optical properties. Besides, the computed changes in dipole moment between the ground state and crucial excited state for  $\text{Ge}_5\text{AM}_3$  clusters lies in the range of 1.05 to 2.34 au where the highest value of 2.34 au is observed for  $\text{Ge}_5\text{K}_3$  while the lowest value of 1.05 au is obtained for the  $\text{Ge}_5\text{Li}_3$  cluster. A similar decreasing trend of change in dipole moment is observed for the  $\text{Ge}_9\text{AM}_5$  clusters. The value of excited-state dipole moment for the  $\text{Ge}_9\text{AM}_5$  series lie in the range of 0.62 to 1.86 au. However, the computed values of the excited-state dipole moment are increasing with the increased size of alkali metals within clusters. Finally, the  $\text{Ge}_{10}\text{AM}_3$  series of clusters show further decreased values of change in dipole moment. As a result of the fascinating electronic features of clusters examined, increased optical and nonlinear optical properties might be expected.

### 3.6 Static nonlinear optical properties

The alkali-like superatom clusters  $\text{Ge}_5\text{AM}_3$ ,  $\text{Ge}_9\text{AM}_5$ , and  $\text{Ge}_{10}\text{AM}_3$  examined here have an excess electron nature. As a result, large optical and nonlinear optical (NLO) responses are reasonable predictions. Literature reveals that compounds and clusters with excess electrons characteristics are significantly adopted for triggering nonlinear optical response.<sup>19,36,39,56–65</sup> Hence, the calculated polarizability ( $\alpha_o$ ), hyperpolarizability ( $\beta_o$ ), second hyperpolarizability ( $\gamma_o$ ), and associated electronic parameters are computed and given in Table 3. The calculated values of polarizability (linear optical response) of  $\text{Ge}_5\text{AM}_3$  lie in the range of  $3.70 \times 10^{-23}$  to  $5.3 \times 10^{-23}$  esu. Similarly, the computed values of polarizability ( $\alpha_o$ ) for  $\text{Ge}_9\text{AM}_5$  series are significantly enhanced and lie in the range of  $6.5 \times 10^{-23}$  to  $1.9 \times 10^{-21}$  esu. Alternatively, the obtained values of polarizability of  $\text{Ge}_{10}\text{AM}_3$  series are slightly smaller than those of  $\text{Ge}_9\text{AM}_5$  and lie in range of  $60 \times 10^{-24}$  to  $71 \times 10^{-24}$  au. The increasing trend of polarizability may be seen as the size of alkali metals increases (Li to K). Overall, the highest value of  $1.9 \times 10^{-21}$  esu is obtained for F where the lowest value of  $37 \times 10^{-24}$  esu is observed for A. Furthermore, the significant polarizability values obtained demonstrate the amount of polarity within the examined clusters. Asymmetric distribution of charges and electronic densities inside clusters also contributed to the higher linear optical response.

Furthermore, the calculated values of static hyperpolarizability ( $\beta_o$ ) lie in the range of  $3.44 \times 10^{-29}$  to  $8.99 \times 10^{-26}$  esu. The calculated static first and second hyperpolarizabilities values are significant. Hyperpolarizability values in the proposed superalkali clusters follow the order  $\text{Ge}_9\text{AM}_5 > \text{Ge}_5\text{AM}_3 > \text{Ge}_{10}\text{AM}_3$ . The hyperpolarizability values obtained for the  $\text{Ge}_5\text{M}_3$  series rise monotonically with alkali metal size. The highest value of  $3.41 \times 10^{-28}$  esu is observed for the C cluster while the lowest value ( $3.44 \times 10^{-29}$  esu) is calculated for the A cluster. Similarly, the obtained values of the  $\beta_o$  for the  $\text{Ge}_9\text{AM}_5$  series range from  $1.80 \times 10^{-28}$ – $8.99 \times 10^{-26}$  esu. With the increased metal size and the number of alkali metals in the  $\text{Ge}_9\text{AM}_5$  clusters, there is a huge increase in  $\beta_o$  values. In particular, the  $\text{Ge}_9\text{K}_5$  shows a remarkable  $\beta_o$  value ( $8.99 \times 10^{-26}$



**Table 3** Polarizability ( $\alpha_o$  in  $\times 10^{-24}$  esu), first static hyperpolarizability ( $\beta_o$  in  $\times 10^{-33}$  esu) scattering hyperpolarizability ( $\beta_{vec}$  in  $\times 10^{-33}$  esu), static second hyperpolarizability ( $\gamma_o$  in  $\times 10^{-40}$  esu), HOMO–LUMO gaps ( $E_{H-L}$  in au), and vertical ionization potential (VIP in au) of  $Ge_5AM_3$ ,  $Ge_9AM_5$  and  $Ge_{10}AM_3$  superalkali clusters

Superalkalis	$\alpha_o$	$\beta_o$	$\beta_{vec}$	$\gamma_o$	$E_{H-L}$	VIP
<b><math>Ge_5AM_3</math></b>						
$Ge_5Li_3$ (A)	$3.7 \times 10^{-23}$	$3.44 \times 10^{-29}$	$3.39 \times 10^{-30}$	$1.37 \times 10^{-34}$	4.04	5.49
$Ge_5Na_3$ (B)	$4.5 \times 10^{-23}$	$1.01 \times 10^{-27}$	$9.94 \times 10^{-30}$	$5.5 \times 10^{-34}$	3.25	4.69
$Ge_5K_3$ (C)	$5.3 \times 10^{-23}$	$3.41 \times 10^{-28}$	$2.97 \times 10^{-29}$	$2.80 \times 10^{-33}$	2.77	3.91
<b><math>Ge_9AM_5</math></b>						
$Ge_9Li_5$ (D)	$6.5 \times 10^{-23}$	$1.80 \times 10^{-28}$	$1.81 \times 10^{-29}$	$4.07 \times 10^{-34}$	3.89	4.36
$Ge_9Na_5$ (E)	$3.6 \times 10^{-22}$	$1.57 \times 10^{-26}$	$1.57 \times 10^{-26}$	$2.15 \times 10^{-30}$	1.34	2.81
$Ge_9K_5$ (F)	$1.9 \times 10^{-21}$	$8.99 \times 10^{-26}$	$8.99 \times 10^{-27}$	$7.68 \times 10^{-34}$	0.79	2.15
<b><math>Ge_{10}AM_3</math></b>						
$Ge_{10}Li_3$ (G)	$6.0 \times 10^{-23}$	$1.88 \times 10^{-29}$	$1.88 \times 10^{-29}$	$2.26 \times 10^{-34}$	3.73	4.98
$Ge_{10}Na_3$ (H)	$6.8 \times 10^{-23}$	$3.87 \times 10^{-29}$	$3.87 \times 10^{-29}$	$3.87 \times 10^{-34}$	3.16	4.34
$Ge_{10}K_3$ (I)	$7.1 \times 10^{-23}$	$4.57 \times 10^{-29}$	$4.57 \times 10^{-29}$	$7.68 \times 10^{-34}$	2.45	3.50

esu) which may be attributed to the larger size of alkali metal (K). In comparison, the  $Ge_{10}AM_3$  ( $AM = Li, Na, \text{ and } K$ ) clusters have range of  $1.88 \times 10^{-29}$  to  $4.57 \times 10^{-29}$ , which is lower than the  $Ge_9AM_5$  and  $Ge_5AM_3$  clusters. In our designed and studied clusters the hyperpolarizability response is quite larger than previously reported  $Li_nF$  ( $n = 2-5$ ) superalkali clusters,<sup>39</sup> and  $M_2OCN$  &  $M_2NCO$  ( $M = Li, Na, K$ ) clusters.<sup>64</sup> Excess electron nature might account for considerable hyperpolarizability response found in these clusters. Furthermore, the studied fabulous electronic properties contribute to the hyperpolarizabilities values. As a result, decreased  $E_{H-L}$  gaps and ionization potential (IP) with increasing alkali metals (AM) size ultimately prompt the  $\beta_o$  response.

We used a conventional two model with the sum-over-state (SOS) method to develop a full understanding of hyperpolarizability and its governing factors. The two-level model can be written as follows:  $\beta_{cl} = \Delta\mu \times f_o / \Delta E^3$

Where the  $\Delta\mu$ ,  $f_o$ , and  $\Delta E$  are changes in dipole moment, oscillator strength, and excitation energy for crucial excitation (excitation with maximum oscillator strength). From the above model, one can observe that  $\beta_{cl}$  has a direct relation with change in dipole moment and oscillator strength ( $f_o$ ) while it is inversely related with cubic of excitation energy ( $\Delta E$ ). The obtained values of  $\beta_{cl}$  range from  $1.03 \times 10^{-29}$ – $1.90 \times 10^{-27}$  esu (Table 4). The  $Ge_9AM_5$  has the largest  $\beta_{cl}$  values in the examined clusters series, which is comparable to  $\beta_o$ . For the first series ( $Ge_5AM_3$ ), the  $\beta_{cl}$  is increased with an increase in  $\Delta\mu$  and oscillator strength. In this series,  $Ge_5K_3$  shows a significant  $\beta_{cl}$  response which may be attributed to its noticeable change in dipole moment (2.34 au) and small excitation energy (1.58 eV). As a result, excitation energy ( $E$ ) is considered to be extremely vital in impacting hyperpolarizability response. A similar trend is observed for the second series ( $Ge_9AM_5$ ) where the  $Ge_9Na_5$  shows a notable value ( $1.90 \times 10^{-27}$  esu) of  $\beta_{cl}$  which is due to small excitation energy (transition energy) and higher change in dipole moment (2.49 au). Likewise,  $\beta_{cl}$  values for the  $Ge_{10}AM_3$  series, there is an increase  $\beta_{cl}$  with reduced excitation energy ( $\Delta E$ ). Hence, the excitation energy is deciding factor in

triggering the hyperpolarizability response from the two-level model where its effect is inversely related to  $\beta_{cl}$ . Furthermore, the estimated  $\beta_o$  and  $\beta_{cl}$  values are highly correlated, providing additional insight into the hyperpolarizability response. From the plotted graph (Fig. 4), one can observe that overall, the  $\beta_{cl}$  values increase dramatically for the  $Ge_9Na_5$  cluster.

Projection of hyperpolarizability on dipole moment vector is also evaluated through  $\beta_{vec}$  simulations. The  $\beta_{vec}$  is a vector part of hyperpolarizability and is very important to characterize the nonlinearity of molecules and clusters. The calculated  $\beta_{vec}$  values are given in Table 3. From Table 3, the observed  $\beta_{vec}$  response of designed clusters strongly correlates with total hyperpolarizability which indicates the dipole moment has the same direction projection of hyperpolarizability ( $\beta_o$ ). Furthermore, the quite comparable values of first hyperpolarizabilities with  $\beta_{vec}$  also indicate that the charge transfer is parallel to the

**Table 4** Computed hyperpolarizability from the two-level model ( $\beta_{cl}$  in  $\times 10^{-33}$  esu), change in dipole moment ( $\Delta\mu$  in au), excitation energy ( $\Delta E$  in eV), oscillator strength ( $f_o$  in au) hyper Rayleigh scattering ( $\beta_{HRS}$  in  $\times 10^{-33}$  esu), and depolarization ratio (DR in au) of superalkali clusters

Superalkalis	$\beta_{cl}$	$\Delta\mu$	$\Delta E$	$f_o$	$\beta_{HRS}$	DR
<b><math>Ge_5AM_3</math></b>						
$Ge_5Li_3$ (A)	$1.03 \times 10^{-29}$	1.05	2.16	0.05	$1.31 \times 10^{-29}$	6.87
$Ge_5Na_3$ (B)	$3.11 \times 10^{-29}$	1.14	1.67	0.04	$4.23 \times 10^{-29}$	5.61
$Ge_5K_3$ (C)	$9.79 \times 10^{-29}$	2.34	1.58	0.16	$1.32 \times 10^{-28}$	6.41
<b><math>Ge_9AM_5</math></b>						
$Ge_9Li_5$ (D)	$2.90 \times 10^{-30}$	0.62	1.69	0.01	$1.13 \times 10^{-29}$	2.44
$Ge_9Na_5$ (E)	$1.90 \times 10^{-27}$	2.49	0.01	0.002	$9.61 \times 10^{-27}$	2.41
$Ge_9K_5$ (F)	$9.83 \times 10^{-28}$	1.86	0.75	0.06	$5.03 \times 10^{-26}$	2.45
<b><math>Ge_{10}AM_3</math></b>						
$Ge_{10}Li_3$ (G)	$1.54 \times 10^{-30}$	0.62	1.87	0.01	$1.21 \times 10^{-29}$	2.37
$Ge_{10}Na_3$ (H)	$1.79 \times 10^{-30}$	0.65	2.02	0.21	$2.08 \times 10^{-29}$	2.45
$Ge_{10}K_3$ (I)	$9.64 \times 10^{-31}$	0.49	1.86	0.11	$2.73 \times 10^{-29}$	2.57



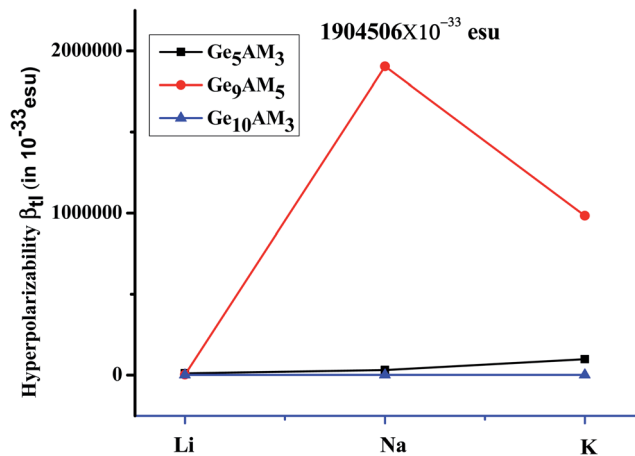


Fig. 4 Representation of  $\beta_H$  for  $\text{Ge}_5\text{AM}_3$ ,  $\text{Ge}_9\text{AM}_5$ , and  $\text{Ge}_{10}\text{AM}_3$  superalkali clusters.

molecular dipole moments. The resemblance of  $\beta_o$  and  $\beta_{\text{vec}}$  also suggests that these clusters can be synthesized in laboratory.

We also carried out calculations for estimation of static second hyperpolarizability ( $\gamma_o$ ) which is a third rank tensor ( $\chi^3$ ). The obtained values of  $\gamma_o$  for the  $\text{Ge}_5\text{AM}_3$  range from  $1.37 \times 10^{-34}$ – $2.80 \times 10^{-33}$  esu which shows an increasing trend with the increased size of alkali metals. Similarly, for the second series ( $\text{Ge}_9\text{AM}_5$ ), the  $\gamma_o$  response increases up to  $2.15 \times 10^{-30}$  esu for E cluster. The  $\gamma_o$  values for the  $\text{Ge}_{10}\text{AM}_3$  superalkali clusters, on the other hand, decrease considerably. Clusters with a higher number of alkali metals (AM) have a substantial  $\gamma_o$  response. Likewise, the  $\gamma_o$  response for the  $\text{Ge}_{10}\text{AM}_3$  clusters lie in the range of  $2.26 \times 10^{-34}$  to  $7.68 \times 10^{-34}$  esu and a slight increase is observed with growing alkali metals size. Hence, the  $\gamma_o$  values vary in order of  $\text{Ge}_9\text{AM}_5 > \text{Ge}_5\text{AM}_3 > \text{Ge}_{10}\text{AM}_3$ .

### 3.7 Hyper Rayleigh scattering measurement ( $\beta_{\text{HRS}}$ )

The hyperpolarizability of nonlinear optical molecules can be determined using hyper-Rayleigh scattering. The  $\beta_{\text{HRS}}$  is a widely used method for determining the nonlinear optical characteristics of centrosymmetric molecules with zero dipole moment. At the same level of theory, we theoretically evaluated the  $\beta_{\text{HRS}}$  response for these clusters. Overall, the calculated highest value ( $5.03 \times 10^{-26}$  esu) of  $\beta_{\text{HRS}}$  is obtained for  $\text{Ge}_9\text{K}_5$  while the lowest value  $1.13 \times 10^{-29}$  esu is observed for D. For the  $\text{Ge}_5\text{AM}_3$  series  $\beta_{\text{HRS}}$  lie in the range of  $1.31 \times 10^{-29}$  esu to  $1.32 \times 10^{-28}$  esu, and are increased with size (Li to K). In the  $\text{Ge}_9\text{AM}_5$  series, the usual trend of beta-HRS value of  $\text{Ge}_9\text{Li}_5$  may be attributed to the small size of Li-atom. Similarly, other nonlinear optical parameters for  $\text{Ge}_9\text{Li}_5$  are also small. It has been reported in the literature previously that dominating factor changes from structure to structure (and it ultimately leads to irregular trends). However, factors affecting the  $\beta_{\text{HRS}}$  response might be the same as total hyperpolarizability values. A similar increasing trend of  $\beta_{\text{HRS}}$  with the size of metal (AM) can be seen for the second series of clusters ( $\text{Ge}_9\text{AM}_5$ ). Furthermore,  $\beta_{\text{HRS}}$  values do not increase with clusters size,

rather these show dependence upon the size of and the number of alkali metals. As a result, the  $\beta_{\text{HRS}}$  values for the  $\text{Ge}_{10}\text{AM}_3$  become slightly smaller, ranging from  $1.22 \times 10^{-29}$  to  $2.73 \times 10^{-29}$  esu. Interestingly, the  $\text{Ge}_9\text{K}_5$  exhibits a significant HRS response which suggests better NLO properties. Additionally, the depolarization ratio (DR) is higher for  $\text{Ge}_5\text{AM}_3$  clusters and increases up to 6.87 au for  $\text{Ge}_5\text{Li}_3$ .

**3.7.1 Dynamic nonlinear optical properties.** The frequency-dependent NLO properties are the fundamental molecular parameters that are required for the description of many nonlinear optical phenomena. The theoretical understanding and accurate determination of the frequency-dependent hyperpolarizabilities  $\beta(\omega)$  and second hyperpolarizabilities  $\gamma(\omega)$  are therefore crucial to classify nonlinearity of materials. The frequency-dependent NLO response is estimated at dispersion frequencies of 532 and 1064 nm, and we calculated electro-optic pockel's effect (EOPE) with  $\beta(-\omega; \omega, 0)$  and electric field induced second harmonic generation (EFISHG) with  $\beta(-2\omega; \omega, \omega)$  at applied frequency. The obtained values of electro-optical pockel's effect (EOPE) for  $\text{Ge}_5\text{AM}_3$  clusters at dispersion frequency of 532 nm range from. The EOPE effect is much pronounced at a small dispersion frequency of 532 nm. Similarly, the obtained dynamic hyperpolarizabilities  $\beta(-2\omega; \omega, \omega)$  values noticeably at smaller frequencies. Overall, the highest values ( $3.54 \times 10^{-26}$  esu) of EOPE is obtained for C whereas the lowest value of  $3.02 \times 10^{-28}$  esu is observed for D (Table 5). The is a gradual increase in  $\beta(\omega)$  with an increased size of alkali metals metal. Both EOPE and SHG show significant values at smaller applied frequencies, and their values slightly decrease at higher dispersion frequency (1064 nm).

The calculated frequency-dependent second hyperpolarizability  $\gamma(\omega)$  that includes dc-Kerr  $\gamma^{\text{dc-Kerr}}(\omega) = \gamma(-\omega; \omega, 0, 0)$  and second harmonic generation with  $\gamma^{\text{ESHG}}(\omega) = \gamma(-2\omega; \omega, \omega, 0)$  are calculated at the same level of theory. The calculated values of dynamic second hyperpolarizability are

Table 5 Frequency-dependent hyperpolarizability  $\beta$  in form of electro-optic pockel's effect (EOPE)  $\beta(-\omega; \omega, 0)$  in  $\times 10^{-33}$  esu, and electric field induced second harmonic generation (EFISHG) with  $\beta(2 - \omega; \omega, \omega)$  in  $\times 10^{-33}$  esu at  $\omega = 532$  nm and  $\omega = 1064$  nm

Superalkalis	$\omega = 0.0856$ au (532 nm)		$\omega = 0.0428$ au (1064 nm)	
	$\beta(-\omega; \omega, 0)$	$\beta(-2\omega; \omega, 0)$	$\beta(-\omega; \omega, 0)$	$\beta(-2\omega; \omega, 0)$
<b><math>\text{Ge}_5\text{AM}_3</math></b>				
$\text{Ge}_5\text{Li}_3$ (A)	$3.28 \times 10^{-27}$	$4.42 \times 10^{-27}$	$6.99 \times 10^{-29}$	$1.81 \times 10^{-28}$
$\text{Ge}_5\text{Na}_3$ (B)	$1.29 \times 10^{-27}$	$3.63 \times 10^{-27}$	$2.50 \times 10^{-28}$	$3.72 \times 10^{-28}$
$\text{Ge}_5\text{K}_3$ (C)	$3.54 \times 10^{-26}$	$1.30 \times 10^{-26}$	$2.24 \times 10^{-28}$	$9.50 \times 10^{-28}$
<b><math>\text{Ge}_9\text{AM}_5</math></b>				
$\text{Ge}_9\text{Li}_5$ (D)	$3.02 \times 10^{-29}$	$3.28 \times 10^{-29}$	$7.86 \times 10^{-29}$	$1.47 \times 10^{-30}$
$\text{Ge}_9\text{Na}_5$ (E)	$7.68 \times 10^{-28}$	$4.42 \times 10^{-27}$	$1.56 \times 10^{-26}$	$2.94 \times 10^{-27}$
$\text{Ge}_9\text{K}_5$ (F)	$6.39 \times 10^{-27}$	$1.04 \times 10^{-26}$	$4.93 \times 10^{-29}$	$1.39 \times 10^{-27}$
<b><math>\text{Ge}_{10}\text{AM}_3</math></b>				
$\text{Ge}_{10}\text{Li}_3$ (G)	$9.67 \times 10^{-29}$	$1.98 \times 10^{-28}$	$2.24 \times 10^{-29}$	$6.99 \times 10^{-29}$
$\text{Ge}_{10}\text{Na}_3$ (H)	$5.71 \times 10^{-28}$	$3.71 \times 10^{-28}$	$2.85 \times 10^{-29}$	$5.62 \times 10^{-29}$
$\text{Ge}_{10}\text{K}_3$ (I)	$1.21 \times 10^{-27}$	$1.04 \times 10^{-27}$	$5.87 \times 10^{-29}$	$2.42 \times 10^{-28}$



**Table 6** Frequency-dependent second hyperpolarizability with dc-Kerr effect  $\gamma(-\omega;\omega,0,0)$  and electric field induced second harmonic generation (ESHG)  $\gamma(-2-\omega;\omega,\omega,0)$  in  $\times 10^{-40}$  esu at  $\omega = 532$  and 1064 nm

Superalkalis	$\omega = 0.0856$ au (532 nm)		$\omega = 0.0428$ au (1064 nm)	
	$\gamma(-\omega;\omega,0,0)$	$\gamma(-2\omega;\omega,\omega,0)$	$\gamma(-\omega;\omega,0,0)$	$\gamma(-2\omega;\omega,\omega,0)$
<b>Ge<sub>5</sub>AM<sub>3</sub></b>				
Ge <sub>5</sub> Li <sub>3</sub> (A)	$7.84 \times 10^{-31}$	$1.37 \times 10^{-30}$	$3.39 \times 10^{-34}$	$1.40 \times 10^{-30}$
Ge <sub>5</sub> Na <sub>3</sub> (B)	$1.30 \times 10^{-32}$	$1.64 \times 10^{-31}$	$2.45 \times 10^{-33}$	$2.31 \times 10^{-33}$
Ge <sub>5</sub> K <sub>3</sub> (C)	$5.43 \times 10^{-36}$	$2.52 \times 10^{-29}$	$7.37 \times 10^{-32}$	$2.09 \times 10^{-31}$
<b>Ge<sub>9</sub>AM<sub>5</sub></b>				
Ge <sub>9</sub> Li <sub>5</sub> (D)	$1.36 \times 10^{-33}$	$5.74 \times 10^{-32}$	$3.16 \times 10^{-32}$	$1.19 \times 10^{-33}$
Ge <sub>9</sub> Na <sub>5</sub> (E)	$1.76 \times 10^{-29}$	$8.80 \times 10^{-30}$	$1.58 \times 10^{-31}$	$1.03 \times 10^{-32}$
Ge <sub>9</sub> K <sub>5</sub> (F)	$5.23 \times 10^{-32}$	$2.53 \times 10^{-32}$	$2.15 \times 10^{-30}$	$3.76\ 747\ 508 \times 10^{-32}$
<b>Ge<sub>10</sub>AM<sub>3</sub></b>				
Ge <sub>10</sub> Li <sub>3</sub> (G)	$8.45 \times 10^{-32}$	$1.24 \times 10^{-31}$	$3.24 \times 10^{-40}$	$5.28 \times 10^{-34}$
Ge <sub>10</sub> Na <sub>3</sub> (H)	$1.22 \times 10^{-32}$	$6.84 \times 10^{-34}$	$1.72 \times 10^{-32}$	$2.41 \times 10^{-33}$
Ge <sub>10</sub> K <sub>3</sub> (I)	$5.23 \times 10^{-32}$	$2.53 \times 10^{-32}$	$2.15 \times 10^{-30}$	$3.76 \times 10^{-32}$

given in Table 6. The calculated dc-Kerr constant and EFSHG are higher at 532 nm and their values slightly decreased at higher dispersion frequency (1064 nm). Likewise, Ge<sub>9</sub>AM<sub>5</sub> and Ge<sub>10</sub>AM<sub>3</sub> are also larger at a small dispersion frequency of 532 nm. Hence, the studied clusters offer tremendous dynamic NLO properties at the smaller external applied frequency.

## 4 Conclusion

In the summary, we explored the zintl-based superalkali for geometric, electronic and nonlinear optical properties. The studied zintl superalkali clusters Ge<sub>5</sub>AM<sub>3</sub>, Ge<sub>9</sub>AM<sub>5</sub>, and Ge<sub>10</sub>AM<sub>3</sub> (AM = Li, Na, K) belong to excess electron compounds. These are superalkali clusters as their calculated vertical ionization potential (VIP) values are smaller than Li atom (5.39 eV). The calculated significant VIP values suggest their electronic stability. The calculated chemical hardness ( $\eta$ ) lie in the range of 2.13 to 4.51 eV, and Ge<sub>9</sub>AM<sub>5</sub> shows the higher softness among the series. There is a significant charge (positive in magnitude) on alkali metals, and the charge is transferred from alkali to Ge-atom. The charge is transferred from alkali metals to Ge-atoms within the clusters. There is a notable reduction in  $E_{H-L}$  (0.79–4.04 eV) which reveals their conductive applications. These clusters are completely transparent in the deep UV region, and show absorption maxima ( $\lambda_{max}$ ) at the longer wavelength. Being excess electron compounds these clusters shows remarkable hyperpolarizability response up to  $8.99 \times 10^{-26}$  esu where the static second hyperpolarizability ( $\gamma_0$ ) value recorded up to  $2.15 \times 10^{-30}$  esu for Ge<sub>9</sub>AM<sub>5</sub> clusters. The adopted two-level model study reveals the controlling factors of hyperpolarizability. The obtained significant  $\beta_H$  value of  $1.90 \times 10^{-27}$  esu may attributed to smaller excitation energy (0.01 eV) The frequency-dependent hyperpolarizabilities and second hyperpolarizabilities values are much higher at smaller dispersion frequencies ( $\omega = 532$  nm). Moreover, the hyper Rayleigh scattering ( $\beta_{HRS}$ ) increases up to  $5.03 \times 10^{-27}$  esu for the Ge<sub>9</sub>K<sub>5</sub> cluster.

## Conflicts of interest

There are no conflicts to declare.

## Acknowledgements

The authors acknowledge the financial and technical support from the Higher Education Commission of Pakistan and COMSATS University, Abbottabad Campus.

## References

- C. Chen and G. Liu, Recent advances in nonlinear optical and electro-optical materials, *Annu. Rev. Mater. Sci.*, 1986, **16**(1), 203–243.
- S. J. Qin and T. A. Badgwell, An overview of nonlinear model predictive control applications, in *Nonlinear model predictive control*, Springer, 2000, pp. 369–392.
- T. H. Maiman, Stimulated optical radiation in ruby, *Nature*, 1960, **187**(4736), 493–494.
- V. M. Agranovich, Y. N. Gartstein and M. Litinskaya, Hybrid resonant organic–inorganic nanostructures for optoelectronic applications, *Chem. Rev.*, 2011, **111**(9), 5179–5214.
- J. Guo, *et al.*, 2D GeP as a novel broadband nonlinear optical material for ultrafast photonics, *Laser Photon. Rev.*, 2019, **13**(9), 1900123.
- H. Yu, N. Z. Koocher, J. M. Rondinelli and P. S. Halasyamani, Pb<sub>2</sub>BO<sub>3</sub>I: A Borate Iodide with the Largest Second-Harmonic Generation (SHG) Response in the KBe<sub>2</sub>BO<sub>3</sub>F<sub>2</sub> (KBBF) Family of Nonlinear Optical (NLO) Materials, *Angew. Chem. Int. Ed.*, 2018, **57**(21), 6100–6103.
- A. Lukic, *et al.*, Endoscopic fiber probe for nonlinear spectroscopic imaging, *Optica*, 2017, **4**(5), 496–501.
- B. Wang, I. Riemann, H. Schubert, D. Schweitzer, K. König and K. Halbhuber, Multiphoton microscopy for monitoring



- intratissue femtosecond laser surgery effects, *Lasers Surg. Med.*, 2007, **39**(6), 527–533.
- 9 M. Nakano, *et al.*, Second Hyperpolarizabilities ( $\gamma$ ) of Bisimidazole and Bistriazole Benzenes: Diradical Character, Charged State, and Spin State Dependences, *J. Phys. Chem. A*, 2006, **110**, 4238.
- 10 Y.-K. Lee, S.-J. Jeon and M. Cho, Molecular polarizability and first hyperpolarizability of octupolar molecules: donor-substituted triphenylmethane dyes, *J. Am. Chem. Soc.*, 1998, **120**(42), 10921–10927.
- 11 L. Karki, F. W. Vance, J. T. Hupp, S. M. LeCours and M. J. Therien, Electronic Stark Effect Studies of a Porphyrin-Based Push–Pull Chromophore Displaying a Large First Hyperpolarizability: State-Specific Contributions to  $\beta$ , *J. Am. Chem. Soc.*, 1998, **120**(11), 2606–2611.
- 12 S.-J. Wang, Y.-F. Wang and C. Cai, Multidecker Sandwich Complexes VnBenn+1 ( $n = 1, 2, 3$ ) as Stronger Electron Donor Relative to Ferrocene for Designing High-Performance Organometallic Second-Order NLO Chromophores: Evident Layer Effect on the First Hyperpolarizability and Two-Dimensional N, *J. Phys. Chem. C*, 2015, **119**, 5589.
- 13 R. L. Zhong, H. L. Xu, Z. R. Li and Z. M. Su, Role of excess electrons in nonlinear optical response, *J. Phys. Chem. Lett.*, 2015, **6**(4), 612–619.
- 14 P. S. Halasyamani and W. Zhang, *inorganic materials for UV and deep-UV nonlinear-optical applications*, ACS Publications, 2017.
- 15 X.-H. Li, L. Zhang, X.-L. Zhang, B.-L. Ni, C.-Y. Li and W.-M. Sun, Designing a new class of excess electron compounds with unique electronic structures and extremely large nonlinear optical responses, *New J. Chem.*, 2020, **44**, 6411–6419.
- 16 H. M. He, *et al.*, Effects of the Cage Number and Excess Electron Number on the Second Order Nonlinear Optical Response in Molecular All-Metal Electride Multicage Chains, *J. Phys. Chem. C*, 2017, **121**(45), 25531–25540.
- 17 F. Ma, *et al.*, Lithium salt electride with an excess electron pair - A class of nonlinear optical molecules for extraordinary first hyperpolarizability, *J. Phys. Chem. A*, 2008, **112**(45), 11462–11467.
- 18 W. M. Sun, *et al.*, Designing Alkalides with Considerable Nonlinear Optical Responses and High Stability Based on the Facially Polarized Janus all-cis-1,2,3,4,5,6-Hexafluorocyclohexane, *Organometallics*, 2017, **36**(17), 3352–3359.
- 19 A. Ahsan and K. Ayub, Adamantane based alkaline earthides with excellent nonlinear optical response and ultraviolet transparency, *Opt. Laser Technol.*, 2020, **129**, 106298.
- 20 A. K. Srivastava and N. Misra, M<sub>2</sub>X (M = Li, Na; X = F, Cl): the smallest superalkali clusters with significant NLO responses and electride characteristics, *Mol. Simul.*, 2016, **42**(12), 981–985.
- 21 J. L. Dye, Electrides: Early Examples of Quantum Confinement, *Acc. Chem. Res.*, 2009, **42**(10), 1564–1572.
- 22 R. H. Huang, J. L. Eglin, S. Z. Huang, L. E. H. McMills and J. L. Dye, Complexation of the cations of six alkalides and an electride by mixed crown ethers, *J. Am. Chem. Soc.*, Oct. 1993, **115**(21), 9542–9546.
- 23 A. Ahsan and K. Ayub, Extremely large nonlinear optical response and excellent electronic stability of true alkaline earthides based on hexaammine complexant, *J. Mol. Liq.*, 2020, **297**, 111899.
- 24 F. Ullah, N. Kosar, K. Ayub and T. Mahmood, Superalkalis as a source of diffuse excess electrons in newly designed inorganic electrides with remarkable nonlinear response and deep ultraviolet transparency: A DFT study, *Appl. Surf. Sci.*, 2019, **483**, 1118–1128.
- 25 J. Iqbal, R. Ludwig and K. Ayub, Phosphides or nitrides for better NLO properties? A detailed comparative study of alkali metal doped nano-cages, *Mater. Res. Bull.*, 2017, **92**, 113–122.
- 26 F. Ullah, N. Kosar, A. Ali, T. Mahmood and K. Ayub, Alkaline earth metal decorated phosphide nanoclusters for potential applications as high performance NLO materials; A first principle study, *Phys. E*, 2020, **118**, 113906.
- 27 A. S. Rad and K. Ayub, Nonlinear optical and electronic properties of Cr-, Ni-, and Ti-substituted C<sub>20</sub> fullerenes: a quantum-chemical study, *Mater. Res. Bull.*, 2018, **97**, 399–404.
- 28 A. S. Rad and K. Ayub, Substitutional doping of zirconium-, molybdenum-, ruthenium-, and palladium: An effective method to improve nonlinear optical and electronic property of C<sub>20</sub> fullerene, *Comput. Theor. Chem.*, 2017, **1121**, 68–75.
- 29 N. Kosar, K. Shehzadi, K. Ayub and T. Mahmood, Theoretical study on novel superalkali doped graphdiyne complexes: Unique approach for the enhancement of electronic and nonlinear optical response, *J. Mol. Graphics Modell.*, 2020, 107573.
- 30 H. Sajid, K. Ayub and T. Mahmood, Exceptionally high NLO response and deep ultraviolet transparency of superalkali doped macrocyclic oligofuran rings, *New J. Chem.*, 2020, **44**(6), 2609–2618.
- 31 B. G. A. Brito, G.-Q. Hai and L. Cândido, Analysis of the ionization potentials of small superalkali lithium clusters based on quantum Monte Carlo simulations, *Chem. Phys. Lett.*, 2018, **708**, 54–60.
- 32 E. Cochran, G. Muller and G. Meloni, Stability and bonding of new superalkali phosphide species, *Dalton Trans.*, 2015, **44**(33), 14753–14762.
- 33 T. Zhao, Q. Wang and P. Jena, Rational design of superalkalis and their role in CO<sub>2</sub> activation, *Nanoscale*, 2017, **9**(15), 4891–4897.
- 34 N. Hou, Y.-Y. Wu, H.-S. Wu and H.-M. He, The important role of superalkalis on the static first hyperpolarizabilities of new electrides: Theoretical investigation on superalkali-doped hexamethylenetetramine (HMT), *Synth. Met.*, 2017, **232**, 39–45.
- 35 W.-M. Sun, *et al.*, A theoretical study on superalkali-doped nanocages: unique inorganic electrides with high stability, deep-ultraviolet transparency, and a considerable



- nonlinear optical response, *Dalton Trans.*, 2016, **45**(17), 7500–7509.
- 36 K. Shehzadi, K. Ayub and T. Mahmood, Theoretical study on design of novel superalkalis doped graphdiyne: A new donor–acceptor (D- $\pi$ -A) strategy for enhancing NLO response, *Appl. Surf. Sci.*, 2019, **492**, 255–263.
- 37 W. M. Sun, L. T. Fan, Y. Li, J. Y. Liu, D. Wu and Z. R. Li, On the potential application of superalkali clusters in designing novel alkalides with large nonlinear optical properties, *Inorg. Chem.*, 2014, **53**(12), 6170–6178.
- 38 J. J. Wang, *et al.*, The interaction between superalkalis (M 3 O, M = Na, K) and a C 20 F 20 cage forming superalkali electride salt molecules with excess electrons inside the C 20 F 20 cage: Dramatic superalkali effect on the nonlinear optical property, *J. Mater. Chem.*, 2012, **22**(19), 9652–9657.
- 39 A. K. Srivastava and N. Misra, Nonlinear optical behavior of LinF (n = 2–5) superalkali clusters, *J. Mol. Model.*, 2015, **21**(12), 1–5.
- 40 D. Hou, D. Wu, W. M. Sun, Y. Li and Z. R. Li, Evolution of structure, stability, and nonlinear optical properties of the heterodinuclear CNLin (n = 1–10) clusters, *J. Mol. Graphics Modell.*, 2015, **59**, 92–99.
- 41 M. J. T. Oliveira, P. V. C. Medeiros, J. R. F. Sousa, F. Nogueira and G. K. Gueorguiev, Optical and magnetic excitations of metal-encapsulating Si cages: A systematic study by time-dependent density functional theory, *J. Phys. Chem. C*, 2014, **118**(21), 11377–11384.
- 42 M. I. A. Oliveira, R. Rivelino, F. de Brito Mota and G. K. Gueorguiev, Optical properties and quasiparticle band gaps of transition-metal atoms encapsulated by silicon cages, *J. Phys. Chem. C*, 2014, **118**(10), 5501–5509.
- 43 S. Scharfe, F. Kraus, S. Stegmaier, A. Schier and T. F. Fässler, Zintl ions, cage compounds, and intermetalloid clusters of group 14 and group 15 elements, *Angew. Chem. Int. Ed.*, 2011, **50**(16), 3630–3670.
- 44 S. Giri, G. N. Reddy and P. Jena, Organo-Zintl Clusters [P7R4]: A New Class of Superalkalis, *J. Phys. Chem. Lett.*, 2016, **7**(5), 800–805.
- 45 G. N. Reddy, A. V. Kumar, R. Parida, A. Chakraborty and S. Giri, Zintl superalkalis as building blocks of supersalts, *J. Mol. Model.*, 2018, **24**(11), 1–13.
- 46 W. Sun, Decorating Zintl polyanions with alkali metal cations: A novel strategy to design superatom cations with low electron affinity, *J. Alloys Compd.*, 2018, **740**, 400–405.
- 47 M. J. Frisch *et al.*, *Gaussian 09 (Revision A. 02)* [Computer software], Gaussian Inc., Wallingford CT, 2009.
- 48 T. Yanai, D. P. Tew and N. C. Handy, A new hybrid exchange–correlation functional using the Coulomb-attenuating method (CAM-B3LYP), *Chem. Phys. Lett.*, 2004, **393**(1–3), 51–57.
- 49 M. T. P. Beerepoot, D. H. Friese, N. H. List, J. Kongsted and K. Ruud, Benchmarking two-photon absorption cross sections: performance of CC2 and CAM-B3LYP, *Phys. Chem. Chem. Phys.*, 2015, **17**(29), 19306–19314.
- 50 M. Li, J. R. Reimers, M. J. Ford, R. Kobayashi and R. D. Amos, Accurate prediction of the properties of materials using the CAM-B3LYP density functional, *J. Comput. Chem.*, 2021, 1486–1497.
- 51 P. A. Limacher, K. V. Mikkelsen and H. P. Luthi, On the Accurate Calculation of Polarizabilities and Second Hyperpolarizabilities of Polyacetylene Oligomer Chains using the CAM-B3LYP Density Functional, *J. Chem. Phys.*, 2009, **130**, 194114.
- 52 A. Ahsin and K. Ayub, Remarkable electronic and NLO properties of bimetallic superalkali clusters: a DFT study, *J. Nanostruct. Chem.*, 2021, 1–17.
- 53 M. B. Oviedo, N. V. Ilawe and B. M. Wong, Polarizabilities of  $\pi$ -conjugated chains revisited: improved results from broken-symmetry range-separated DFT and new CCSD (T) benchmarks, *J. Chem. Theory Comput.*, 2016, **12**(8), 3593–3602.
- 54 R. Vijayaraj, V. Subramanian and P. K. Chattaraj, Comparison of Global Reactivity Descriptors Calculated Using Various Density Functionals: A QSAR Perspective, *J. Chem. Theory Comput.*, Oct. 2009, **5**(10), 2744–2753.
- 55 S. K. Pathak, *et al.*, Experimental (FT-IR, FT-Raman, UV and NMR) and quantum chemical studies on molecular structure, spectroscopic analysis, NLO, NBO and reactivity descriptors of 3,5-Difluoroaniline, *Spectrochim. Acta, Part A*, 2015, **135**, 283–295.
- 56 A. Ahsin, A. Ali and K. Ayub, Alkaline earth metals serving as source of excess electron for alkaline earth metals to impart large second and third order nonlinear optical response; A DFT study, *J. Mol. Graphics Modell.*, 2020, **101**, 107759.
- 57 F. Ullah, N. Kosar, K. Ayub, M. A. Gilani and T. Mahmood, Theoretical study on a boron phosphide nanocage doped with superalkalis: novel electrides having significant nonlinear optical response, *New J. Chem.*, 2019, **43**(15), 5727–5736.
- 58 N. Kosar, *et al.*, Significant nonlinear optical response of alkaline earth metals doped beryllium and magnesium oxide nanocages, *Mater. Chem. Phys.*, 2020, **242**, 122507.
- 59 A. S. Rad and K. Ayub, Change in the electronic and nonlinear optical properties of Fullerene through its incorporation with Sc-, Fe-, Cu-, and Zn transition metals, *Appl. Phys. A*, 2019, **125**(6), 430.
- 60 S. Sajjad, A. Ali, T. Mahmood and K. Ayub, Journal of Molecular Graphics and Modelling Janus alkaline earthides with excellent NLO response from sodium and potassium as source of excess electrons; a first principles study, *J. Mol. Graphics Modell.*, 2020, **100**, 107668.
- 61 F. Ullah, K. Ayub and T. Mahmood, Remarkable second and third order nonlinear optical properties of organometallic C6Li6–M3O electrides, *New J. Chem.*, 2020, **44**, 9822–9829.
- 62 K. Ayub, Are phosphide nano-cages better than nitride nano-cages? A kinetic, thermodynamic and non-linear optical properties study of alkali metal encapsulated X 12 Y 12 nano-cages, *J. Mater. Chem. C*, 2016, **4**(46), 10919–10934.



Paper

- 63 S. Munsif, *et al.*, Remarkable nonlinear optical response of alkali metal doped aluminum phosphide and boron phosphide nanoclusters, *J. Mol. Liq.*, 2018, **271**, 51–64.
- 64 A. Ahsin and K. Ayub, Theoretical Investigation of Superalkali Clusters M<sub>2</sub>OCN and M<sub>2</sub>NCO (where M= Li, Na, K) as Excess Electron System with Significant Static and Dynamic Nonlinear optical response, *Opt.*, 2020, 166037.
- 65 A. Ahsin and K. Ayub, Superalkali-based alkalides Li<sub>3</sub>O@[12-crown-4]M (where M= Li, Na, and K) with remarkable static and dynamic NLO properties; A DFT study, *Mater. Sci. Semicond. Process.*, 2022, **138**, 106254.

